Physics Guided Neural Networks for Spatio-temporal Super-resolution of Turbulent Flows

Abstract

Direct numerical simulation (DNS) of turbulent flows is computationally expensive and cannot be applied to flows with large Reynolds numbers. Low-resolution large eddy simulation (LES) is a popular alternative, but it is unable to capture all of the scales of turbulent transport accurately. Reconstructing DNS from low-resolution LES is critical for large-scale simulation in many scientific and engineering disciplines, but it poses many challenges to existing super-resolution methods due to the complexity of turbulent flows and computational cost of generating frequent LES data. We propose a physics-guided neural network for reconstructing frequent DNS from sparse LES data by enhancing its spatial resolution and temporal frequency. Our proposed method consists of a partial differential equation (PDE)-based recurrent unit for capturing underlying temporal processes and a physics-guided super-resolution model that incorporates additional physical constraints. We demonstrate the effectiveness of both components in reconstructing the Taylor-Green Vortex using sparse LES data. Moreover, we show that the proposed recurrent unit can preserve the physical characteristics of turbulent flows by leveraging the physical relationships in the Navier-Stokes equation.

1 INTRODUCTION

Understanding turbulence is the key to our comprehension of many natural and technological processes in engineering, science, and medicine research. Since the pioneering work of Orszag and Patterson (Orszag and Patterson [1986]), direct numerical simulation (DNS) of the Navier-Stokes equations have been widely regarded as the computational method with the highest fidelity in capturing the dynamics of turbulent flows. DNS is essentially a brute force numerical solution of the unsteady governing equations of fluid flow, and thus can be very computationally expensive. Straightforward estimates indicate that simulation of an incompressible flow with Reynolds number $\mathrm{Re} = \mathcal{O}(10^5)$ within a domain of size of $\mathcal{O}\left[(100\ell)^3\right]$ would require about *a century* of CPU time on a 1 teraflop computer! A practical alternative, the large eddy simulation (LES) concentrates on the larger scale eddies and models the subgrid-scale transport. By this filtering, LES can be conducted on coarser grids as compared to those required by DNS. The penalty, understandably, is that LES-generated data are of lower accuracy compared to DNS.

Machine learning, especially super-resolution (SR) methods (Park et al. [2003]), has shown great success in reconstructing high-resolution data in a variety of commercial applications. The power of these models comes mainly from the use of convolutional network layers (Albawi et al. [2017]), which can extract the spatial texture features and transform them through complex non-linear mappings to recover high-resolution data. From the earliest end-to-end convolution-based SR model (Dong et al. [2014]), many investigators have added skip-connections in SR models (Zhang et al. [2018a], Duong et al. [2021], Dai et al. [2019], Zhang et al. [2018b], Ahn et al. [2018], Tai et al. [2017]) to bypass redundant low-resolution information and promote the stability of optimizing deep networks. Moreover, advances in adversarial learning allow preservation of high-level features extracted from target high-resolution images through a separate discriminator network (Ledig et al. [2017], Chen et al. [2018], Wang et al. [2018a,b], Karras et al. [2017], Upadhyay and Awate [2019], Cheng et al. [2021], Wenlong et al. [2021]). Given their success in computer vision, SR models have also been applied to reconstruct turbulence data (Fukami et al. [2019], Obiols-Sales et al. [2021], Deng et al. [2019], Stengel et al. [2020], Venkatesh et al. [2021], Xie et al. [2018], Fukami et al. [2020], Liu et al. [2020]).

However, existing SR methods face several challenges when they are applied for reconstructing turbulent flows. Turbu-

Submitted to the 38th Conference on Uncertainty in Artificial Intelligence (UAI 2022). **To be used for reviewing only**.

lent flows involve multiple physical variables and often exhibit complex dynamic patterns, i.e., multiple physical variables evolve and interact at different scales. In the absence of underlying physical processes, pure data-driven SR models require a large number of training samples to capture the correct physics. Due to the substantial computational cost in simulating turbulent flows, high-fidelity DNS data are rarely available, and even the generation of high-quality LES at a lower resolution can be expensive. Hence, low-resolution LES data cannot be frequently generated for a variety of simulation scenarios. When trained with limited data at discrete time steps (i.e., when both LES and DNS are available), these models can have degraded performance because they may learn spurious patterns between sparse observations, and such patterns are often not generalizable.

In this paper, we propose a new physics-guided neural network framework for spatial and temporal super-resolution. The idea is to leverage underlying physical relationships to guide the learning of generalizable spatial and temporal patterns in the reconstruction process. In particular, our framework consists of two components, physics-guided recurrent unit (PRU) and physics-guided super resolution model (PGSR). The PRU structure is designed based on the underlying partial differential equation (PDE), and is responsible for capturing the temporal dynamics of turbulent flows from sparse data. The PGSR model incorporates additional physical constraints to improve the reconstruction from the available LES data. Our evaluation of the Taylor-Green Vortex data (Brachet et al. [1984]) has demonstrated the superiority of PRU and PGSR in modeling the turbulent flows. We also verify that the proposed method can preserve the physical properties of turbulent flows.

Our contributions can be summarized as:

- We propose innovative physics-guided PRU and PGSR architectures to capture the temporal and spatial patterns of the turbulent flows, respectively.
- We design a unified neural network framework combining PGSR and PRU to effectively simulate and reconstruct high-resolution frequent turbulent flows.
- We evaluate our model in a series of experiments. The experimental results demonstrate that our approaches have significant superiority compared with existing methods in both DNS simulation from historical data and DNS reconstruction from sparse LES data.

2 PROBLEM DEFINITION

Our objective is to reconstruct frequent high-resolution flow data from low-resolution and sparse LES data. In particular, we consider a general three-dimensional vortex flow over space and time $\boldsymbol{Q}(x, y, z, t)$, where (x, y, z) denotes the spatial coordinates, t represents the time step (in seconds), and $\boldsymbol{Q}(x, y, z, t)$ consists of multiple variables that describe turbulent transport, such as the velocity along with different directions and the thermodynamic pressure. We represent low-resolution LES data as $\boldsymbol{Q}^{LR}(x, y, z, t)$, which are available at sparse time steps, e.g., starting from a time step t_0, the LES is generated with a time interval of d at $\{t_0, t_0 + d, t_0 + 2d, ...\}$. The flow variables in $\boldsymbol{Q}(x, y, z, t)$ also follow the Navier-Stokes equation, which governs the transport of these variables in space (x, y, z) and time (t). Boundary conditions are specified near the boundary of the domain to describe the interaction of the flow with the external environment. More details about the flow dataset will be provided in Section 4.1.

3 METHOD

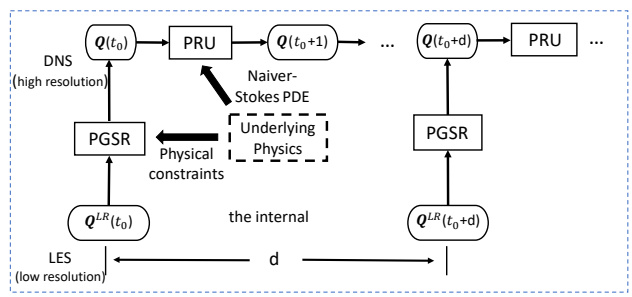

Figure 1: The proposed physics-guided neural networks framework combining PRU and PGSR for reconstructing turbulent flows $\boldsymbol{Q}$.

Our proposed framework consists of two structural components, PGSR and PRU, which are illustrated in Fig. 1. Starting from an initial time step t_0, the proposed method will follow a two-step process: (i) the PGSR model is used to reconstruct high-resolution $\boldsymbol{Q}(x, y, z, t)$ when low-resolution LES data are available. (ii) Then PRU is used to estimate $\boldsymbol{Q}(x, y, z, t + 1)$ from $\boldsymbol{Q}(x, y, z, t)$ until the next LES sample is available. In the following, we will describe the two components, PRU and PGSR.

3.1 PHYSICS-GUIDED RECURRENT UNIT (PRU)

Physical variables $\boldsymbol{Q}$ in turbulent flows interact with each other and evolve at different speeds for different locations. Temporal neural network models, e.g., long-short term memory (LSTM) (Hochreiter and Schmidhuber [1997]), have sophisticated structures and thus heavily rely on large representative training data that are sampled at the high temporal frequency to capture the underlying continuous patterns over time. Given sparse and limited LES data, we develop the PRU structure as a more accurate and reliable way to predict the future flow variables by leveraging the continuous physical relationship described by the underlying PDE. This helps bridge the gap between discrete data samples and continuous flow dynamics. The proposed PRU structure is also generally applicable to many dynamical systems with governing PDEs.

Most PDEs can be represented in the form of $\boldsymbol{Q}_t = \boldsymbol{f}(t, \boldsymbol{Q}; \theta)$, where $\boldsymbol{Q}_t$ is the temporal derivative of $\boldsymbol{Q}$, and $\boldsymbol{f}(t, \boldsymbol{Q}; \theta)$ is a non-linear function (parameterized by coefficient θ) that summarizes the current value of $\boldsymbol{Q}$ and its spatial context. For example, the incompressible Navier-Stokes equation for the velocity field can be expressed as:

$$\boldsymbol{f}(\boldsymbol{Q}) = \frac{-1}{\rho}\nabla p + \nu \Delta \boldsymbol{Q} - (\boldsymbol{Q}.\nabla)\boldsymbol{Q}, \tag{1}$$

where ρ, p, and ν denote the fluid density, the thermodynamic pressure, and the viscosity, respectively. Since the function $\boldsymbol{f}(\boldsymbol{Q})$ in the Navier-Stokes equation is independent of time t, we omit the independent variable t in the function $\boldsymbol{f}(\cdot)$. Here p is treated as a known variable, and $\theta = \{\rho, \nu\}$.

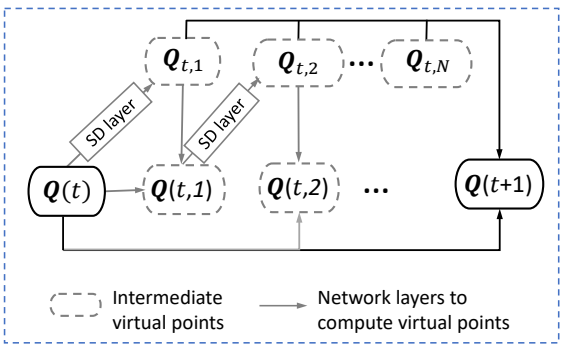

Figure 2: Diagram for the physical recurrent unit.

The PRU structure is inspired by the classical numerical Runge–Kutta (RK) methods (Butcher [2007]), which have been used in temporal discretization for the approximate solutions of differential equations. As shown in Fig. 2, the central idea of PRU is to interpolate virtual intermediate variables and create smaller intervals between two time steps which facilitate refining the gradient of flow variables over time. Starting from a time step t, PRU estimates $N-1$ intermediate state variables $\boldsymbol{Q}(t,1)$, ..., $\boldsymbol{Q}(t,N-1)$ and N intermediate temporal derivatives $\boldsymbol{Q}_{t,1}$, ..., $\boldsymbol{Q}_{t,N}$ before reaching the next step $t+1$.

In particular, PRU interpolates intermediate state variables by iteratively following a two-step process: for n from 1 to N, (i) PRU first estimates the temporal derivative $\boldsymbol{Q}_{t,n} = \boldsymbol{f}(\boldsymbol{Q}(t, n-1))$ at the previous intermediate flow state $\boldsymbol{Q}(t, n-1)$, and $\boldsymbol{Q}(t, 0) = \boldsymbol{Q}(t)$. We will discuss more details about how to compute the function $\boldsymbol{f}(\cdot)$ later. (ii) Then PRU computes the next intermediate state variable $\boldsymbol{Q}(t, n)$ by moving the flow data $\boldsymbol{Q}(t)$ along the direction of obtained temporal derivatives. In our tests, we follow the most popular 4th order RK method for computing the three intermediate state variables, as follows:

$$\begin{aligned} \boldsymbol{Q}(t,1) &= \boldsymbol{Q}(t) + \Delta t \frac{\boldsymbol{Q}_{t,1}}{2}, \\ \boldsymbol{Q}(t,2) &= \boldsymbol{Q}(t) + \Delta t \frac{\boldsymbol{Q}_{t,2}}{2}, \\ \boldsymbol{Q}(t,3) &= \boldsymbol{Q}(t) + \Delta t \boldsymbol{Q}_{t,3}, \end{aligned} \tag{2}$$

The temporal derivative $\boldsymbol{Q}_{t,4}$ is then computed from the last intermediate point, as $\boldsymbol{f}(\boldsymbol{Q}(t,3))$. The 4th order RK method has the total accumulated error of $O(\Delta t^4)$, where Δt represents the time interval between consecutive time steps.

Finally, PRU combines all the intermediate temporal derivatives as a composite gradient to predict the flow variables at the next time step $\boldsymbol{Q}(t+1)$, as follows:

$$\text{PRU}(\hat{\boldsymbol{Q}}(t+1)|\boldsymbol{Q}(t)) = \boldsymbol{Q}(t) + \sum_{n=1}^{N} w_n \boldsymbol{Q}_{t,n}, \tag{3}$$

where $\{w_n\}_{n=1}^{N}$ are the trainable model parameters. Given a series of high-fidelity DNS training data of T time steps, the PRU structure can be trained by minimizing the mean squared error (MSE) between the predicted flow variables and true DNS values, as $\sum_t ||\text{PRU}(\hat{\boldsymbol{Q}}(t+1)|\boldsymbol{Q}(t)) - \boldsymbol{Q}(t+1)||^2/T$.

In the following, we will describe two major issues in computing the function $\boldsymbol{f}(\cdot)$: (i) estimating spatial derivatives in the function $\boldsymbol{f}(\cdot)$, and (ii) preserving boundary conditions. We will also investigate the stability of this method for long-term prediction with a simple case.

3.1.1 Spatial derivative approximation

The proposed PRU evaluates the function $\boldsymbol{f}(\cdot)$ explicitly for estimating the temporal derivatives of intermediate state variables. In many general PDEs (e.g., the Navier-Stokes equation), $\boldsymbol{f}(\boldsymbol{Q})$ contain spatial derivatives of $\boldsymbol{Q}$. One popular approach for evaluating the spatial derivatives is through the finite difference methods (FDMs), which approximate variable derivatives of a function on predefined mesh points by solving algebraic equations containing finite differences and values from nearby points. In particular, the first and second order spatial derivatives (along x dimension) in Eq. 1 can be estimated by FDMs as follows:

$$\begin{aligned} \boldsymbol{Q}_x(x_i, y_j, z_k, t_n) &\approx \frac{\boldsymbol{Q}(x_{i+1}, y_j, z_k, t_n) - \boldsymbol{Q}(x_{i-1}, y_j, z_k, t_n)}{2\Delta x}, \\ \boldsymbol{Q}_{xx}(x_i, y_j, z_k, t_n) &\approx \frac{\boldsymbol{Q}(x_{i+1}, y_j, z_k, t_n) - 2\boldsymbol{Q}(x_i, y_j, z_k, t_n)}{2\Delta x} \\ &\quad + \frac{\boldsymbol{Q}(x_{i-1}, y_j, z_k, t_n)}{2\Delta x}. \end{aligned} \tag{4}$$

The approximation used in FDMs results in an error compared to the exact solution, which can be estimated through Taylor expansions. Instead of using FDMs for every mesh point, we propose to build a spatial difference (SD) layer using convolutional neural network (CNN) layers. The CNN layers have the expressive power to capture the relationships defined in FDMs (Eq. 4) while also being more flexible in learning other non-linear relationships from data.

3.1.2 Boundary Condition and Augmentation

Boundary conditions are critical in turbulent flow simulation as they describe how the turbulent flows interact with the external environment. Here we consider the periodic boundary condition in our flow data. It is defined in a specified periodic domain indicating that it repeats its own values in all directions. The formal definition of a cubic periodic boundary condition is given below:

$$\begin{aligned} \boldsymbol{Q}(L_x, y, z, t) &= \boldsymbol{Q}(R_x, y, z, t), \\ \boldsymbol{Q}(x, L_y, z, t) &= \boldsymbol{Q}(x, R_y, z, t), \\ \boldsymbol{Q}(x, y, R_z, t) &= \boldsymbol{Q}(x, y, R_z, t), \end{aligned} \tag{5}$$

where L_x, L_y, L_z are the three left boundaries with respect with x, y, z coordinates and R_x, R_y, R_z are the three right boundaries with respect with x, y, z coordinates. Standard padding strategies for CNN (e.g., same padding) do not satisfy the periodic value requirement. In order to handle this issue, we make a data augmentation for each of the 6 faces (of the 3D cubic data) with an additional 2 layers of data during the training stage and adopt a 5×5 CNN filter size. The augmented locations will be removed from reconstructed data.

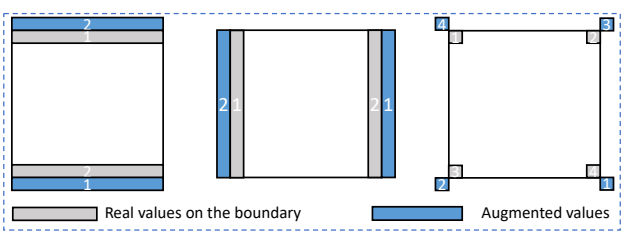

Figure 3: Illustration of data augmentation on a 2-D example. The left diagram represents the up and low boundary augmentation. The middle diagram represents the left and right boundary augmentation. The right diagram represents the corner boundary augmentation. Rectangles carrying identical numbers have the same value.

3.1.3 Stability

The classical 4th order RK suffers from the stability issue if the step size is not properly chosen. Consider a simple scalar example $Q_t = \lambda Q$. The 4th order RK for this equation can be written as

$$Q((n+1)\Delta t) \approx (1 + \lambda\Delta t + \frac{\lambda\Delta t^2}{2} + \frac{\lambda\Delta t^3}{6} + \frac{\lambda\Delta t^4}{24})Q(n\Delta t). \tag{6}$$

Let's denote $R(\Delta t) = 1 + \Delta t + \frac{\Delta t^2}{2} + \frac{\Delta t^3}{6} + \frac{\Delta t^4}{24}$, and we have $Q((n+1)\Delta t) = R(\Delta t)Q(n\Delta t)$. The analytical solution is $Q((n+1)\Delta t) = \exp(\lambda\Delta t)Q(n\Delta t)$, and thus the accumulated error is

$$err_{n+1} = (\exp(\lambda\Delta t) - R(\Delta t))err_n. \tag{7}$$

This indicates that $err_{n+1} = O(\Delta t^5)err_n$ according to Taylor expansion. When the interval d of LES data is large, the accumulated error may get amplified at every time step and then lead to an explosion. Additional complexity arises when f consists of multiple evaluations of spatial derivatives. This requires the access to LES data at a reasonably frequent time interval to avoid significantly large reconstruction errors.

Algorithm 1 The flow of the proposed PRU.

Create and initialize 5×5 filters for 1st and 2nd order spatial derivatives
for $epoch$ = 1 : number of training iterations **do**
  for t = 1 : number of time steps **do**
    Make data augmentation for $\boldsymbol{Q}(t)$ (Section 3.1.2).
    Calculate $\boldsymbol{Q}_{t,1}, \boldsymbol{Q}_{t,2}, \boldsymbol{Q}_{t,3}, \boldsymbol{Q}_{t,4}$ following Eq. 2 and evaluate $\boldsymbol{f}$ accordingly.
    Calculate $\hat{\boldsymbol{Q}}(t+1)$ following Eq. 3 and remove augmented data over boundaries.
    Use the predicted $\hat{\boldsymbol{Q}}(t+1)$ as the input flow data for time $t+1$.
  end for
  Update trainable filters and weights.
end for

3.2 PHYSICS GUIDED SUPER RESOLUTION (PGSR)

The PGSR model aims to incorporate additional physical constraints to regularize the standard super-resolution model. In particular, we consider two important physical constraints, the divergence-free property for the incompressible flow and the zero-mean property for the Taylor-Green Vortex (Brachet et al. [1984]).

First, the incompressible flow follows the divergence-free property in the velocity field. Thus, we can represent the inherent physical relationship of the velocity field as:

$$\nabla \cdot \mathbf{V} = \frac{\partial u}{\partial x} + \frac{\partial v}{\partial y} + \frac{\partial w}{\partial z} = 0, \tag{8}$$

where we represent the velocity vector $\mathbf{V}(\mathbf{x}, t)$ along 3-D dimensions ($\mathbf{x} \equiv x, y, z$) by u, v, and w, respectively. Then we use a second-order central finite difference approximation to estimate the partial derivatives and employ this divergent free property as a physical loss in the training process, as follows:

$$\mathcal{L}_{\text{Phy}} = \sum_{(x,y,z)} \left[\nabla \cdot \hat{\mathbf{V}}(\mathbf{x}, t)\right]^2 / M, \tag{9}$$

where M is the number of spatial locations in the high-resolution data, and $\hat{\mathbf{V}}$ represents the reconstructed velocity field at high resolution. Such physical constraint can help

reduce the search space for model parameters such that the reconstructed high-resolution data follow the divergence-free property which is enforced in incompressible flows.

Second, to preserve the zero-mean property of the in a compressible flow, we also implement an extra network layer by reducing the mean value of reconstructed flows in the generative process $\hat{\boldsymbol{Q}}_0 = g(\hat{\boldsymbol{Q}})$. We do not include the zero-mean constraint directly in the loss function because the obtained model cannot preserve the zero-mean property for the long-term testing phase. On the other hand, direct MSE minimization using $\hat{\boldsymbol{Q}}_0$ as output leads to an unstable training process because the original output $\hat{\boldsymbol{Q}}$ can have arbitrarily large values. Hence, we iteratively train the PGSR model to reduce (i) the gap between $\hat{\boldsymbol{Q}}$ and the true DNS and (ii) the gap between $\hat{\boldsymbol{Q}}$ and its resulted $\hat{\boldsymbol{Q}}_0$, and finally use $\hat{\boldsymbol{Q}}_0$ as the output.

Additionally, we also introduce a degradation process to enforce the consistency between the reconstructed data and the input LES data, similar to Chen et al. [2021]. We create the PGSR model based on the popular SR model SRGAN (Ledig et al. [2017]). The methods we used to include physical constraints can also be used to enhance other SR models.

4 EXPERIMENT

In this section, we evaluate the performance of our method on a Taylor-Green vortex (TGV) (Brachet et al. [1984]) dataset and compare the results with existing well-used methods. We first introduce the dataset used in our tests and discuss the experimental design and evaluation targets. Then we will provide experimental results and our analysis.

4.1 DATASET

We consider a variant of the Taylor-Green vortex (TGV). This is a three-dimensional incompressible flow and is simulated within a box with periodic boundary conditions. The TGV provides a suitable setting for our demonstration as it exhibits several salient features of turbulent transport. In this flow, the original vortex collapses into turbulent worm-like structures which become progressively more turbulent until viscosity eventually dissipates the large scale vortical structures. We compare our proposed method against several existing super-resolution algorithms to reconstruct the DNS data of TGV.

The TGV is produced by a solution of the constant density Navier-Stokes equation:

$$\frac{\partial \mathbf{V}}{\partial t} + (\mathbf{V}.\nabla)\mathbf{V} = \frac{-1}{\rho}\nabla p + \nu \Delta \mathbf{V}. \tag{10}$$

The evolution of the TGV includes enhancement of vorticity stretching and the consequent production of small-scale eddies. Initially, large vortices are placed in a cubic periodic domain of $[-\pi, \pi]$ (in all three-directions), with initial conditions:

$$u(x, y, z, 0) = \sin(x)\cos(y)\cos(z) \tag{11}$$
$$v(x, y, z, t) = -\cos(x)\sin(y)\cos(z) \tag{12}$$
$$w(x, y, z, t) = 0. \tag{13}$$

Then the value of the Reynolds number is set to $Re = 1600$. We have LES and DNS results of TGV at several times steps. For each time step, we consider the three components of the velocity along the x, y, and z axis, denoted by u, v, and w, respectively. Our objective is to reconstruct the DNS results of the velocity field (u, v, w) using LES data. In particular, $\boldsymbol{Q}^{LR}$ represents the LES values of the velocity field while the target $\boldsymbol{Q}$ represents the high-fidelity DNS of the velocity field. Here both LES and DNS data are generated along 65 grid points along the z axis under equal intervals. The LES and DNS are conducted on 32-by-32 and 128-by-128 grid points, respectively, along the xy directions. Hence, the DNS data is of 16 times higher resolution compared to LES data.

4.2 EXPERIMENTAL DESIGN

We train the proposed method using the TGV data from a consecutive 20-seconds period (with 20 time steps) and then apply the trained model to the next 50 seconds' testing data and measure the performance. [1] We evaluate the performance of DNS prediction using two different evaluation metrics, root mean squared error (RMSE) and structural similarity index measure (SSIM) (Wang et al. [2004]). We use RMSE to measure the difference (error) between reconstructed data and target DNS data. The lower value of RMSE indicates better reconstruction performance at the pixel level. SSIM is used to appraise the structural similarity between reconstructed data and target DNS on three aspects: luminance, contrast, and overall structure.

Our evaluations aim to answer several questions as listed below:

E1: *Whether PRU alone can effectively predict the next high-resolution DNS using the previous DNS data?* We will compare PRU with two pure data-driven baseline models, transition model (TM) and recurrent transition model (rTM). The TM method predicts the flow variables $\boldsymbol{Q}(t+1)$ at next step using an UNet-style encoder-decoder convolutional structure from the flow variables $\boldsymbol{Q}(t)$ at the previous time. The rTM method further extends TM with a recurrent layer.

E2: *Whether the predictions made by PRU can preserve physical properties of DNS?* Besides RMSE and SSIM, we

[1] Code for the experiment is available at drive.google.com/drive/folders/11PTaEjsBkgd6PAAYmWH_KDzTg90IvrJn?usp=sharing

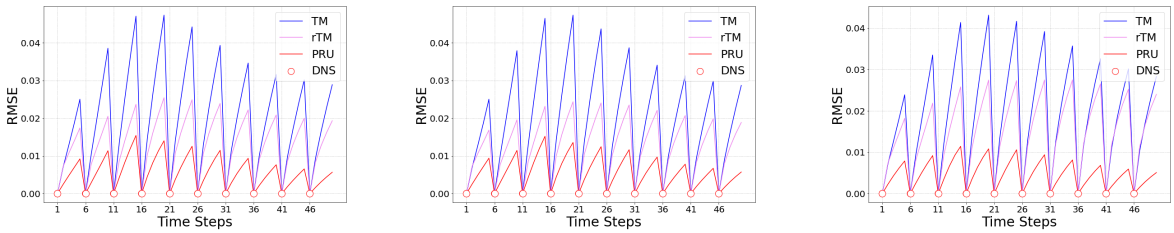

(a) RMSE in u Channel. (b) RMSE in v Channel. (c) RMSE in w Channel.

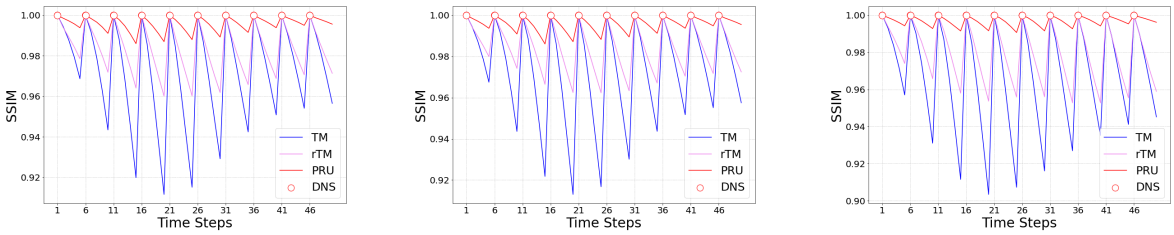

(d) SSIM in u Channel. (e) SSIM in v Channel. (f) SSIM in w Channel.

Figure 4: Change of RMSE/SSIM values produced by different DNS prediction models from the 1st to 50th time steps in a testing period with true DNS data for 5 time steps. (a)-(c) show the changes of RMSE values, and (d)-(f) show the changes of SSIM values for (u,v,w) three different channels.

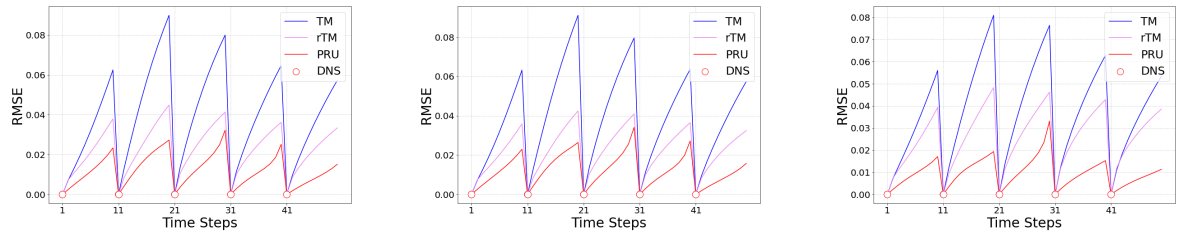

(a) RMSE in u Channel. (b) RMSE in v Channel. (c) RMSE in w Channel.

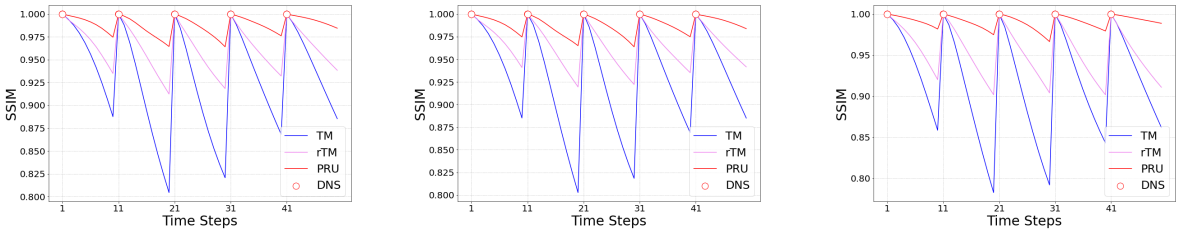

(d) SSIM in u Channel. (e) SSIM in v Channel. (f) SSIM in w Channel.

Figure 5: Change of RMSE/SSIM values produced by different DNS prediction models from the 1st to 50th time steps in a testing period with true DNS data for 10 time steps. (a)-(c) show the changes of RMSE values, and (d)-(f) show the changes of SSIM values for (u,v,w) three different channels.

will measure the turbulent kinetic energy of the predicted flows and compare it with that of the true DNS.

E3: *How is the reconstruction performance combining PRU and PGSR using sparse low-resolution LES data?* We will combine PRU and PGSR (PGSR-PRU) for reconstructing DNS from sparse LES samples. Since we have already compared PRU with other temporal transition models in **E1**, here we compare to a baseline SRGAN-TM, which uses our base SR model SRGAN for reconstructing DNS from LES and use TM to predict DNS when LES is not available. We also compare to another two baselines PGSR (LES) and its extension rPGSR (LES). rPGSR(LES) has another recurrent layer over time. Different from PGSR-PRU and SRGAN-TM, these two methods apply the SR model using LES data

Table 1: DNS prediction performance by RMSE and SSIM. The performance is measured on (u, v, w) channels with DNS interval d as 5 or 10.

	Method	RMSE	SSIM
	TM	(0.019,0.019,0.019)	(0.972,0.973,0.967)
d	rTM	(0.013,0.012,0.015)	(0.983,0.984,0.980)
=5	PRU	(0.005,0.005,0.005)	(0.996,0.996,0.997)
	TM	(0.038,0.038,0.036)	(0.930,0.930,0.917)
d	rTM	(0.022,0.022,0.025)	(0.964,0.966,0.954)
=10	PRU	(0.012,0.012,0.009)	(0.988,0.988,0.991)

at all the time steps, thus can be considered as the upper bound for this test. Our goal is to verify that PGSR-PRU can produce comparable performance with PGSR (LES) and rPGSR (LES).

E4: *How is the reconstruction performance of PGSR compared to other SR methods?* We compare PGSR with two well-used SR methods: RCAN (Zhang et al. [2018a]) and SRGAN (Ledig et al. [2017]). We also compare it with DCS/MS (Fukami et al. [2019]), which is a popular SR approach for turbulent flows reconstruction. Additionally, we compare to a variant of PGSR, termed PGSR-D, which only adds the degradation loss to the SRGAN model without using any physical constraints.

4.3 RESULTS

4.3.1 DNS generation using PRU

Here we assume that we have true DNS data with an interval of d time steps (d = 5 or 10) and we implement PRU and other baselines to predict DNS for the missing time steps. We summarize the performance of PRU and baselines in Table 1 and show their performance change on each channel over time in Figs. 4 and 5. For both cases (with the true DNS interval d set to a larger value 10 or a smaller value 5), PRU produces better performance than baselines over all the time steps. It confirms the effectiveness of PRU in the long-term prediction of DNS from historical flow data (**E1**).

Besides, we compute the kinetic energy of the flow data predicted by PRU and baselines and measure the gap with the kinetic energy of the true DNS data. The proposed PRU reduces the kinetic energy gap with the true DNS by 30% and 67% compared to TM and rTM, respectively. It confirms that PRU can better preserve underlying physical characteristics of turbulent flows (**E2**).

4.3.2 DNS reconstruction using PGSR-PRU

We implement the DNS reconstruction using PGSR-PRU and SRGAN-TM using the LES data for every five time steps (**E3**). As shown in Table 2 and Fig. 6, PGSR-PRU produces better performance than SRGAN-TM. Particularly in the first 15 time steps, it is more clear to see PGSRN-PRU can obtain lower RMSE and higher SSIM values. Fig. 6 also shows that the reconstruction performance gets degraded over time because the LES data have a significant difference with the training period. More interestingly, we notice that PGSR-PRU even outperforms PGSR (LES) and rPGSR (LES). This is because LES data often miss many important physical components compared to the true DNS, which makes SR models difficult to recover flow data directly from LES data. We also show three sets of examples of reconstructed slides of flow data in Fig. 7. It is clear to observe that PGSR-PRU can better capture the detailed flow patterns compared to other methods as it incorporates the underlying Navier-Stokes equation through PRU.

Table 2: Reconstruction performance on (u, v, w) using LES channels by RMSE and SSIM. SRGAN-TM and PGSR-PRU (proposed) are evaluated using sparse LES data with the interval of 5 steps, the upper half is the average results of a total of 50 time steps, the bottom half is the average results of the first 15 time steps.

Method	RMSE	SSIM
PGSR (LES)	(0.112, 0.114, 0.133)	(0.771, 0.774, 0.667)
rPGSR (LES)	(0.114, 0.114, 0.129)	(0.772, 0.773, 0.669)
SRGAN-TM	(0.118,0.115, 0.147)	(0.769, 0.767, 0.647)
PGSR-PRU	(0.111,0.113, 0.128)	(0.782, 0.781, 0.681)
PGSR (LES)	(0.088, 0.088, 0.101)	(0.846, 0.849, 0.801)
rPGSR (LES)	(0.091, 0.086, 0.099)	(0.848, 0.855, 0.811)
SRGAN-TM	(0.091,0.088, 0.105)	(0.848, 0.849, 0.794)
PGSR-PRU	(0.081,0.081, 0.091)	(0.864, 0.866, 0.833)

Table 3: Evaluation of SR models in terms of the reconstruction RMSE and SSIM on (u, v, w) channels using LES data. The performance is measured on the testing data of the first 5 time steps.

Method	RMSE	SSIM
RCAN	(0.061, 0.061, 0.075)	(0.891, 0.891, 0.863)
DCS/MS	(0.085, 0.086, 0.115)	(0.896, 0.897, 0.845)
SRGAN	(0.065, 0.062, 0.067)	(0.901, 0.913, 0.875)
PGSR-D	(0.057, 0.052, 0.053)	(0.914, 0.923, 0.900)
PGSR	(0.053, 0.050, 0.051))	(0.924, 0.935, 0.911)

4.3.3 DNS reconstruction using PGSR

As shown in Table 3, PGSR achieves better performance than other baselines in terms of both RMSE and SSIM. In particular, we can observe the improvement from SRGAN to PGSR-D and from PGSR-D to PGSR. This confirms the effectiveness of the degradation process and the physical constraints used in PGSR (**E4**).

5 CONCLUSION

In this paper, we develop a physics-guided neural network framework for predicting high-resolution flow data at high

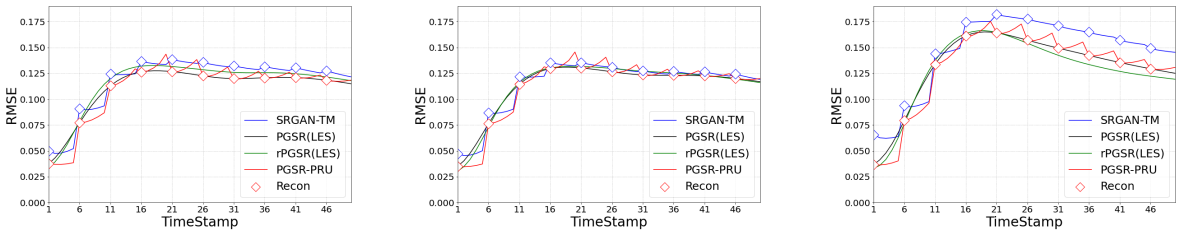

(a) RMSE in u Channel. (b) RMSE in v Channel. (c) RMSE in w Channel.

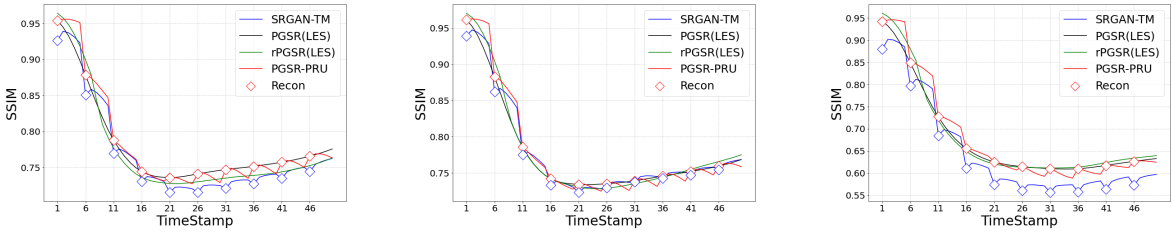

(d) SSIM in u Channel. (e) SSIM in v Channel. (f) SSIM in w Channel.

Figure 6: Change of RMSE/SSIM for different models over time using sparse LES data with the interval of 5 time steps. (a)-(c) show the changes of RMSE values, and (d)-(f) show the changes of SSIM values for (u,v,w) three different channels.

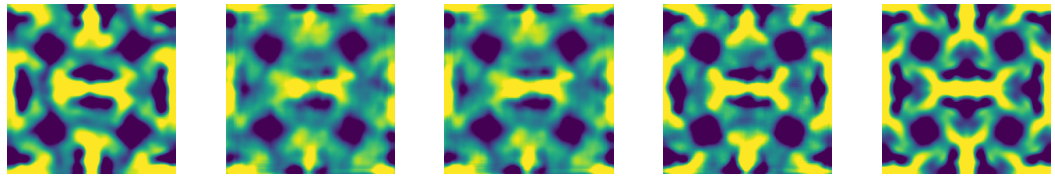

(a) SRGAN-TM (b) PGSR(LES) (c) rPGSR(LES) (d) PGSR-PRU (e) Target DNS

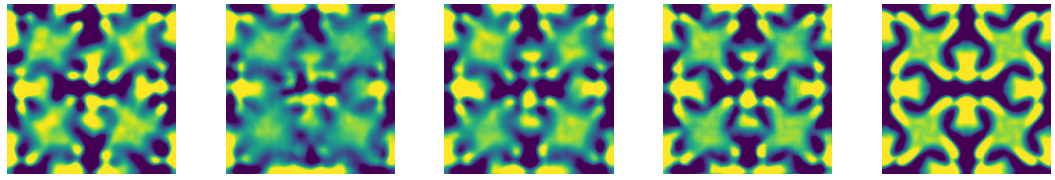

(f) SRGAN-TM (g) PGSR(LES) (h) rPGSR(LES) (i) PGSR-PRU (j) Target DNS.

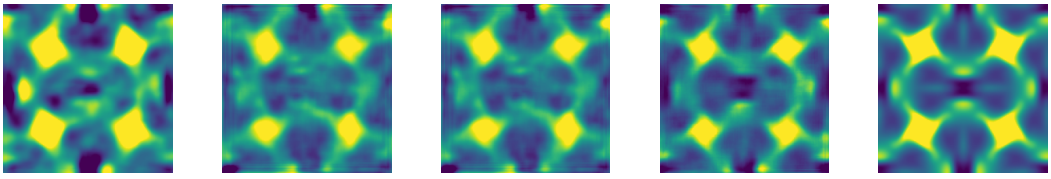

(k) SRGAN-TM (l) PGSR(LES) (m) rPGSR(LES) (n) PGSR-PRU (o) Target DNS

Figure 7: Three example slides of reconstructed w channel (in three rows) along the z dimension with the LES interval of 5 time steps.

temporal frequency. The PRU structure leverages the physical knowledge embodied in the Navier-Stokes equation to capture the flow dynamics over time while the PGSR model incorporates additional physical constraints to improve the reconstruction from the LES data. We have demonstrated the superiority of PRU in predicting future DNS data from historical DNS data. We also show that PGSR-PRU can effectively reconstruct DNS from sparse LES series.

More importantly, the proposed method is generally applicable to many scientific problems with similar properties, e.g., complex temporal dynamics, and the availability of low-resolution simulations with reduced accuracy. The PRU structure can also be used as a building block to enhance existing deep learning models for modeling of complex dynamics with the guidance of known governing PDEs.

BIBLIOGRAPHY

Namhyuk Ahn, Byungkon Kang, and Kyung-Ah Sohn. Fast, accurate, and lightweight super-resolution with cascading residual network, 2018.

Saad Albawi, Tareq Abed Mohammed, and Saad Al-Zawi. Understanding of a convolutional neural network. In *2017 international conference on engineering and technology (ICET)*, pages 1–6. Ieee, 2017.

Marc E Brachet, D Meiron, S Orszag, B Nickel, R Morf, and Uriel Frisch. The taylor-green vortex and fully developed turbulence. *Journal of Statistical Physics*, 34(5):1049–1063, 1984.

John Butcher. Runge-kutta methods. *Scholarpedia*, 2(9): 3147, 2007.

Shengyu Chen, Shervin Sammak, Peyman Givi, Joseph P Yurko, and Xiaowei Jia. Reconstructing high-resolution turbulent flows using physics-guided neural networks. *arXiv preprint arXiv:2109.03327*, 2021.

Yu Chen, Ying Tai, Xiaoming Liu, Chunhua Shen, and Jian Yang. Fsrnet: End-to-end learning face super-resolution with facial priors. In *Proceedings of the IEEE Conference on Computer Vision and Pattern Recognition*, pages 2492–2501, 2018.

Wenlong Cheng, Mingbo Zhao, Zhiling Ye, and Shuhang Gu. Mfagan: A compression framework for memory-efficient on-device super-resolution gan, 2021.

Tao Dai, Jianrui Cai, Yongbing Zhang, Shu-Tao Xia, and Lei Zhang. Second-order attention network for single image super-resolution. In *CVPR*, 2019.

Zhiwen Deng, Chuangxin He, Yingzheng Liu, and Kyung Chun Kim. Super-resolution reconstruction of turbulent velocity fields using a generative adversarial network-based artificial intelligence framework. *Physics of Fluids*, 31(12):125111, 2019.

Chao Dong, Chen Change Loy, Kaiming He, and Xiaoou Tang. Learning a deep convolutional network for image super-resolution. In *European conference on computer vision*, pages 184–199. Springer, 2014.

Vinh Van Duong, Thuc Nguyen Huu, Jonghoon Yim, and Byeungwoo Jeon. A fast and efficient super-resolution network using hierarchical dense residual learning. In *2021 IEEE International Conference on Image Processing (ICIP)*, pages 1809–1813, 2021. doi: 10.1109/ICIP42928.2021.9506786.

Kai Fukami, Koji Fukagata, and Kunihiko Taira. Super-resolution reconstruction of turbulent flows with machine learning. *Journal of Fluid Mechanics*, 870:106–120, 2019.

Kai Fukami, Koji Fukagata, and Kunihiko Taira. Machine-learning-based spatio-temporal super resolution reconstruction of turbulent flows. *Journal of Fluid Mechanics*, 909, Dec 2020. ISSN 1469-7645.

Sepp Hochreiter and Jürgen Schmidhuber. Long short-term memory. *Neural Computation*, 9(8):1735–1780, 1997. doi: 10.1162/neco.1997.9.8.1735.

Tero Karras, Timo Aila, Samuli Laine, and Jaakko Lehtinen. Progressive growing of gans for improved quality, stability, and variation. *arXiv preprint arXiv:1710.10196*, 2017.

Christian Ledig, Lucas Theis, Ferenc Huszár, Jose Caballero, Andrew Cunningham, Alejandro Acosta, Andrew Aitken, Alykhan Tejani, Johannes Totz, Zehan Wang, et al. Photo-realistic single image super-resolution using a generative adversarial network. In *CVPR*, 2017.

Bo Liu, Jiupeng Tang, Haibo Huang, and Xi-Yun Lu. Deep learning methods for super-resolution reconstruction of turbulent flows. *Physics of Fluids*, 2020.

Octavi Obiols-Sales, Abhinav Vishnu, Nicholas Malaya, and Aparna Chandramowlishwaran. Surfnet: Super-resolution of turbulent flows with transfer learning using small datasets. *arXiv preprint arXiv:2108.07667*, 2021.

S. A. Orszag and G. S. Patterson. Numerical simulation of turbulence. In *Statistical Models and Turbulence*, pages 127–147. Springer-Verlag, New York, NY, 1986.

Sung Cheol Park, Min Kyu Park, and Moon Gi Kang. Super-resolution image reconstruction: a technical overview. *IEEE Signal Processing Magazine*, pages 21–36, 2003.

Karen Stengel, Andrew Glaws, Dylan Hettinger, and Ryan N King. Adversarial super-resolution of climatological wind and solar data. *Proceedings of the National Academy of Sciences*, 117(29):16805–16815, 2020.

Ying Tai, Jian Yang, and Xiaoming Liu. Image super-resolution via deep recursive residual network. In *2017 IEEE Conference on Computer Vision and Pattern Recognition (CVPR)*, pages 2790–2798, 2017. doi: 10.1109/CVPR.2017.298.

Uddeshya Upadhyay and Suyash P. Awate. Robust super-resolution gan, with manifold-based and perception loss. In *2019 IEEE 16th International Symposium on Biomedical Imaging (ISBI 2019)*, pages 1372–1376, 2019. doi: 10.1109/ISBI.2019.8759375.

TS Venkatesh, Rajat Srivastava, Pratyush Bhatt, Prince Tyagi, and Raj Kumar Singh. A comparative study of various deep learning techniques for spatio-temporal super-resolution reconstruction of forced isotropic turbulent flows. *arXiv preprint arXiv:2107.03361*, 2021.

Xintao Wang, Ke Yu, Chao Dong, and Chen Change Loy. Recovering realistic texture in image super-resolution by deep spatial feature transform, 2018a.

Xintao Wang, Ke Yu, Shixiang Wu, Jinjin Gu, Yihao Liu, Chao Dong, Yu Qiao, and Chen Change Loy. Esrgan: Enhanced super-resolution generative adversarial networks. In *ECCV Workshops*, 2018b.

Zhou Wang, Alan C Bovik, Hamid R Sheikh, and Eero P Simoncelli. Image quality assessment: from error visibility to structural similarity. *IEEE transactions on image processing*, 13(4):600–612, 2004.

Zhang Wenlong, Liu Yihao, Chao Dong, and Yu Qiao. Ranksrgan: Generative adversarial networks with ranker for image super-resolution. *TPMAI*, 2021. doi: 10.1109/TPAMI.2021.3096327.

You Xie, Erik Franz, Mengyu Chu, and Nils Thuerey. tempogan: A temporally coherent, volumetric gan for super-resolution fluid flow. *ACM Transactions on Graphics (TOG)*, 37(4):1–15, 2018.

Yulun Zhang, Kunpeng Li, Kai Li, Lichen Wang, Bineng Zhong, and Yun Fu. Image super-resolution using very deep residual channel attention networks. In *ECCV*, 2018a.

Yulun Zhang, Yapeng Tian, Yu Kong, Bineng Zhong, and Yun Fu. Residual dense network for image super-resolution, 2018b.